Light Trapping Design in Silicon-Based Solar Cells

Fengxiang Chen and Lisheng Wang
Physics science and technology, Wuhan University of Technology
China

1. Introduction

When the sunlight illuminates the front surface of solar cell, part of the incident energy reflects from the surface, and part of incident energy transmits to the inside of solar cell and converts into electrical energy. Typically, the reflectivity of bare silicon surface is quite higher; more than 30% of incident sunlight can be reflected. In order to reduce the reflection loss on the surface of solar cell, usually the following methods were adopted. One is to corrode and texture the front surface [Gangopadhyay et al., 2007; Ju et al., 2008; Basu et al., 2010; Li et al., 2011], so that incident light can reflect back and forth between the inclined surfaces, which will increase the interaction between incident light and semiconductor surface. The second is coated with a single-layer or multi-layer antireflection film coating [Chao et al., 2010]. Generally, these coatings are very thin, the optical thickness is nearly quarter or half of incident wavelength. Single-layer antireflection coating only has good anti-reflection effect for a single wavelength, so multi-layer antireflection coating is commonly used in high efficiency solar cells, for it has good anti-reflection effect within the wide spectrum of solar radiation. Third, surface plasmons offer a novel way of light trapping by using metal nanoparticles to enhance absorption or light extraction in thin film solar cell structures [Derkacs et al., 2006; Catchpole et al., 2008; Moulin et al.,2008; Nkayama et al.,2008; Losurdo et al.,2009;]. By manipulating their size, the particles can be used as an efficient scattering layer. One of the benefits of this light trapping approach is that the surface area of silicon and surface passivation layer remain the same for a planar cell, so surface recombination losses are not expect to increase.

The above light tapping methods can be used individually or in combination. In the following section we will introduce them in detail.

2. Principle and preparation of textured surface

Textured solar cells can not only increase the absorption of the incident sunlight, it also has many other advantages [Fesquet et al., 2009]. For solar cells, the higher efficiency and the lower cost are always main topic in scientific research. Because the crystalline silicon is non-direct band gap semiconductor material, the absorption of sunlight is relatively weak, the thickness of the solar cell need to exceed a few millimeters to absorb 99% of the solar spectrum, which increased the weight of materials and the production cost, and increased the recombination probability in the bulk, resulting in reduced anti-radiation performance.

The textured surface can be realized by many methods. These methods are different for mono-crystalline silicon and multi-crystalline silicon material. Next, we will introduce the textured methods for silicon solar cells in detail.

2.1 Textured surface for single crystalline silicon

Textured surface is fulfilled on mono-crystalline silicon surface by a selective corrosion. At high temperature, the chemical reaction between silicon and alkali occurs as follows:

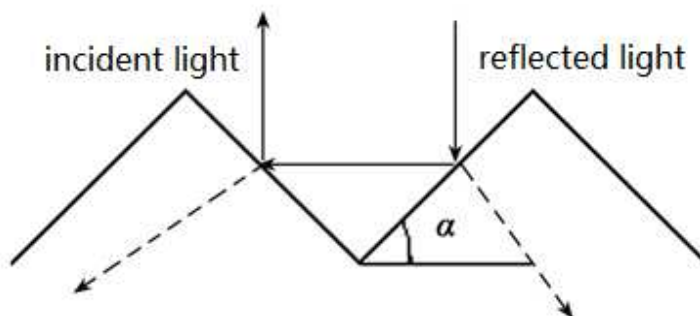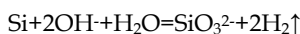$$Si + 2OH^- + H_2O = SiO_3^{2-} + 2H_2 \uparrow$$

Fig. 1. Light trapping by "pyramid" covered at the textured surface.

So hot alkaline solution is usually used to corrode the silicon. For different crystalline faces and crystalline directions, the atoms are arranged differently, so the strength between the atoms is different. According to principles of electrochemical corrosion, their corrosion rate will be different. For {100} planes, the spacing of the adjacent two planes is maximum and the density of covalent bonds is the minimum, so the adjacent layer along the {100} atomic planes are most prone to breakage. On the other hand, atoms within the {111} planes have the minimum distance, and the surface density of covalent bonds is the maximum, which results in that the corrosion rate is the minimum along the <111> direction. Therefore, the corrosion faces revealed by preferential etching solution are (111) planes. After single crystalline silicon material with <100> orientation was corroded preferentially, the pyramids on the surface of mono-crystalline silicon come from the intersection of (111) planes. The "pyramid" structure was shown in Fig. 1.

The low concentrations alkaline solution, such as 1.25% of sodium hydroxide (NaOH) solution is usually used as a selective etching solution, because the corrosion rates of (100) plane and the (111) plane are not the same, the pyramid structure can be obtained on mono-crystalline Si surface, which increased light absorption greatly. In the preparation processes, temperature, ethanol content, NaOH content, and corrosion time are the factors which affect the morphology of the pyramids. Fig.2 shows the SEM pictures of textured surfaces with changes of the corrosion time. It can be seen from Fig.2 that the formation of the pyramids with the corrosion time. For example, after 5min, the pyramid began to appear; after 15min, the silicon surface was covered by small pyramids, and a few have begun to grow up; after 30min, the silicon surface covered with pyramids.
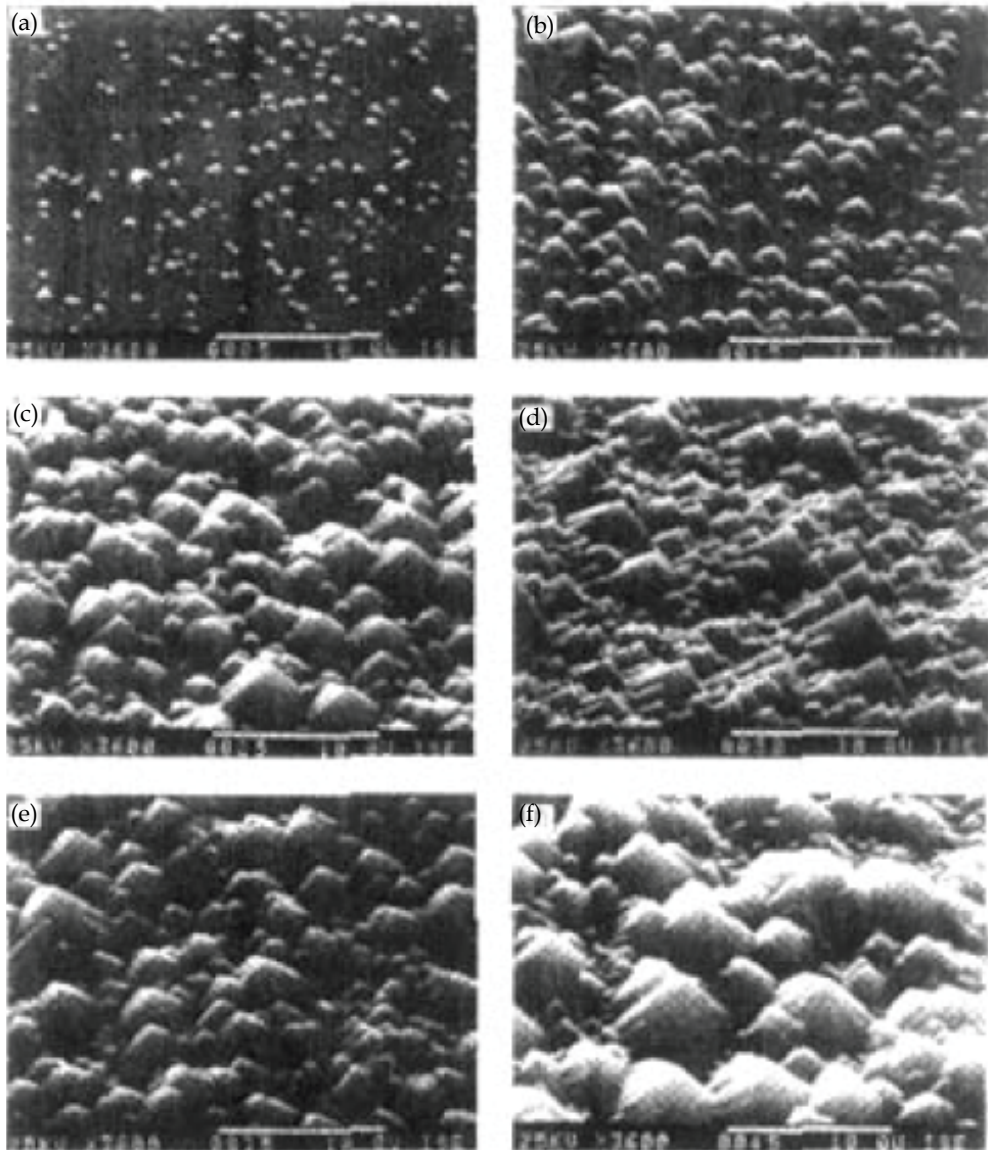
Fig. 2. The SEM pictures of textured surface with the corrosion time, the corrosion time are: (a)5min,(b)15min,(c)25min, (d)30min,(e)35min, (f)40min, respectively.[Wang, 2005]
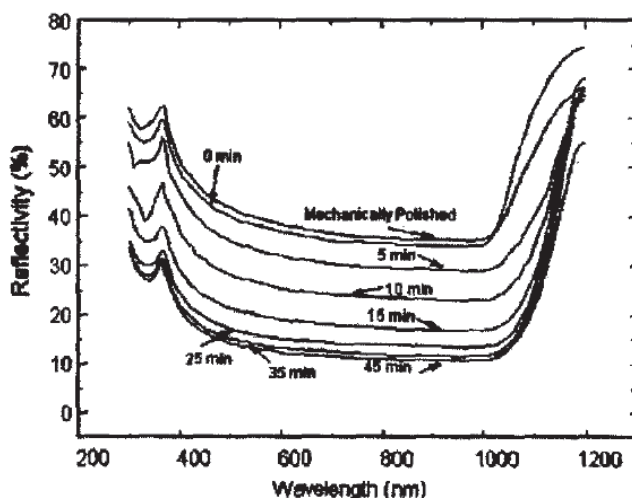
Fig. 3. The reflectivity of silicon wafers after different etching time.[Wang, 2005]

Fig.3 shows the reflectivity of mono-crystalline silicon wafer after different corrosion time (5-45min). We can find that in the visible range (450-1000nm), the reflectivity decreases with increasing corrosion time, the minimum reflectivity is 11%. For the corrosion time is in the 25-45min range, the corresponding reflectivity is nearly 11-14%. If etching time is further increased, no significant change happens in reflectivity.

2.2 Textured surface for polycrystalline silicon

For single crystalline silicon with <100> orientation, the ideal pyramid structure can be etched by NaOH solution. However, for polysilicon, only a very small part of the surface is covered with (100) orientation, so the use of anisotropic etching for textured surface is not feasible. Because the orientations of the grains in polysilicon are arbitrary and alkaline solution such as NaOH or KOH, are anisotropic etching, these can easily result in uneven texture, this alkaline etching method is not suitable for texturing polysilicon. In view of optics, the acid solution (the mixture of HF, HNO_3, and H_2O) and the RIE (reactive ion etching) method are the isotropic surface texture methods for textured surface of polysilicon.

The acid etching solution for polysilicon is mixture of HF, HNO_3 and deionized water mixed by certain percentages, where HNO_3 is used as strong oxidant, so that silicon became SiO_2 after oxidation. The whole silicon surface is covered by dense SiO_2 film after oxidation and this SiO_2 film will protect the silicon from further reaction. HF solution is used as complexing agent and this solution can dissolve SiO_2 film, the resulting $H_2[SiF_6]$ complexes is soluble in water. $H_2[SiF_6]$ is a strong acid, which is stronger than sulfuric acid and easily dissociate in solution. So this reaction is a positive feedback corrosion reaction, with the generation of $H_2[SiF_6]$, and the dissociation from the H^+ concentration increased, then the corrosion rate also increased. If corrosion speed is too fast, the reaction process is difficult to control, leading to poor corrosion. To mitigate the corrosion reaction, by mass action law, reducing the HF concentration can slow the reaction speed. The reaction mechanism is as follows [Yang, 2010]:

$$3Si+4HNO_3=3SiO_2+2H_2O+4NO\uparrow$$

$$SiO_2+6HF=H_2[SiF_6]+2H_2O$$

$$H_2[SiF_6]\Leftrightarrow 2H^++[SiF_6]^{2-}$$
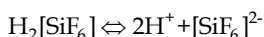
This etching method is isotropic corrosion, which has nothing to do with the orientations of the grains, so it will form a uniform textured surface on the polysilicon surface.

Fig.4 shows the SEM pictures for polysilicon wafers after alkaline etching, acid etching, and first acid corrosion with the second alkaline etching. From Fig.4(a), we can see that after alkaline corrosion the surface is uneven and has more steps. Fig.4(c) shows the morphology of the first acid corrosion with the second alkaline etching, we can find that the pyramid shape and the surface are uneven. So these two surface conditions are not suitable to the sequent screen printing procedure. And SEM picture for acid corrosion is shown in Fig.4 (b). We can get the required thickness by changing the ratio of acid solution and controlling the response speed.

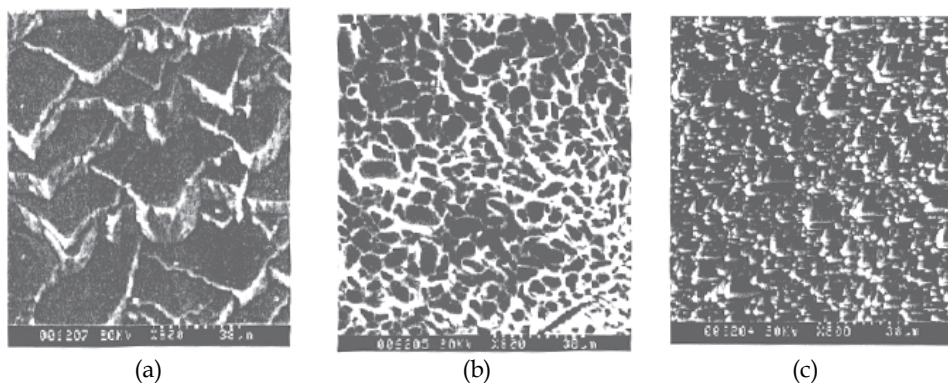(a)   (b)   (c)

Fig. 4. The SEM pictures for (a)polysilicon with alkaline etching;(b)polysilicon with acid etching; (c)polysilicon with first acid etching and second alkaline etching.[Meng, 2001]

Acid etching method for polysilicon has many advantages: firstly, it can remove surface damage layer and texture surface in a very short period of time, this will save the production time; Secondly, the surface after etching is relatively flat and thin, which is easy to make thin battery; Thirdly, NaOH solution is not used, which avoid the contamination from Na ions; and the wafer after the acid corrosion is flat, which is easy to form a relatively flat pn junction, thereby it help to improve the stability of the solar cells; Finally, the flat surface is suitable for the screen printing process and the electrode contact is not prone to break.

The reflectance curves of different polysilicon surfaces are shown in Fig.5. We can found the reflectivity with acid etching is no more than 20% in the range 400-1000nm; after the deposition of silicon nitride anti-reflection coating (ARC), the average reflectivity is less than 10%; and the reflectivity reaches 1% at 600nm wavelength. Thus, the reflection loss with acid etching is very small. In contrast, for the alkaline texture, the reflectivity is relatively higher, while the reflectivity with acid and alkaline double texture is intervenient.
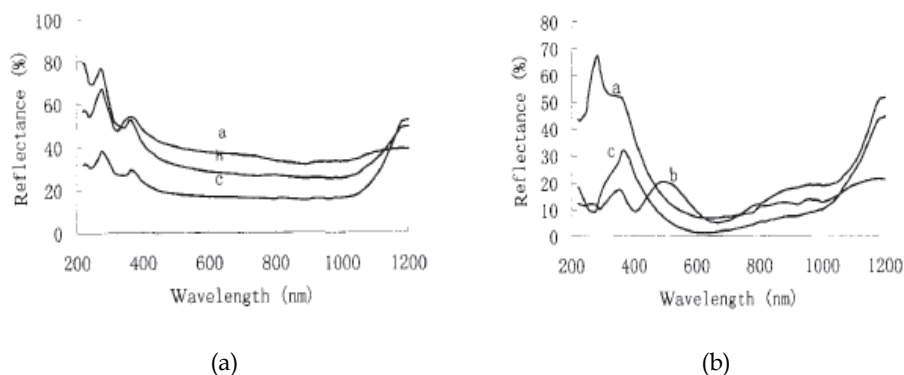
(a) (b)

Fig. 5. Reflectance curves of polysilicon textured with the chemical etching. (a) Without ARC; (b)With SiN ARC. (a-NaOH texturing; b-NaOH after acidic texturing; c-Acidic texturing). [Meng, 2001]

In the RIE preparation process, the gas species, gas flow, pressure and RF power both will influent the etching result. Combined with the gas plasma etching with chlorine gas (Cl_2) and the antireflection coating method, the lower reflectivity can be realized in a wide range of wavelengths. According to [Inomato, 1997], the flow rate of chlorine gas can be easily controlled to adjust the surface aspect ratio, which is helpful to form the similar pyramid structure on the polysilicon surface. The maximum short circuit current and the maximum open circuit voltage can be obtained under the condition the chlorine flow is 4.5sccm. The experimental results show that for the mono-crystalline silicon, the reflectivity is about 1-2% in the 400-1000nm wavelength range. In RIE method, because the chlorine or fluorine was used as etching gas, the influence on the environment should be considered.

The textured structure also has some drawbacks. Firstly, in the production process of pyramids, the acid or alkaline solution is often used, which need to be careful; Secondly, the pyramids on the surface increase the surface area, which reduces the average light intensity. And the multiple reflections on the textured surface will result in the uneven distribution of incident illumination. Both these will affect the open circuit voltage of the solar cell; Thirdly, the textured structure not only decreases the reflectivity, but also increases the absorption of the infrared light. The absorption of infrared light will heat the solar cell and decrease the conversion efficiency of solar cell; seriously it will disable the solar cell.

3. Principle and design of the antireflection coating

3.1 The basic theory of antireflection coating

Most solar cells were coated with an antireflection coating layer to reduce light reflection on the front surface [Kuo et al., 2008]. This is why crystalline silicon solar cells appears to be blue or black while silicon material appears to be grey. A set of optimized and well designed anti-reflection coating on the front surface is an effective way to improve the optical absorption of the solar cell. For certain range in sunlight spectrum, reflectivity on the front surface varies from more than 30% down to less than 5% [Geng et al., 2010], which greatly increase the absorption of incident sunlight energy of the solar cell.

The following figure shows the basic principles of the anti-reflection film. When the reflection of light on second interface returns to the first interface, and if the phase difference between the two lights is 180 degrees, the former will offset the latter to some extent.
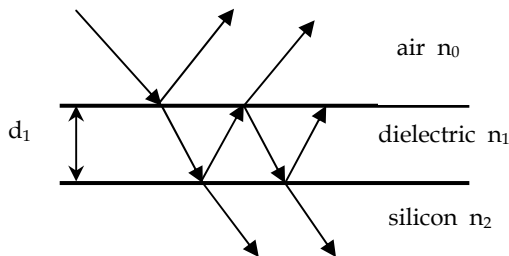

Fig. 6. The principles of the antireflection coating.

When the incident light is normally illuminated, and the silicon material covered with a transparent layer with thickness d_1, the expression of the reflected energy is [Wang, 2001]:

$$R = \frac{r_1^2 + r_2^2 + 2r_1r_2\cos 2\theta}{1 + r_1^2 r_2^2 + 2r_1r_2\cos 2\theta} \tag{1}$$

Where r_1 and r_2 are: $r_1 = \dfrac{n_0 - n_1}{n_0 + n_1}, r_2 = \dfrac{n_1 - n_2}{n_1 + n_2}$

Where n_i represents the diffraction index. The θ is given by:

$$\theta = \frac{2\pi n_1 d_1}{\lambda_0}$$

When $n_1 d_1 = \lambda_0/4$ is fulfilled, the reflectivity has the minimum.

$$R_{\min} = (\frac{n_1^2 - n_0 n_2}{n_1^2 + n_0 n_2})^2$$

If the transparent layer has the greatest antireflective effect, the zero reflectivity R = 0 should be required. This means $n_1 = \sqrt{n_0 n_2}$. Thus for the desired wavelength λ_0 , the refractive index of the antireflective film can be calculated by the above expression. But when the incident wavelength deviates from λ_0 , the reflectivity will increase. Therefore, in order to increase the output of solar cell, the distribution of solar spectrum and the relative spectral response of crystalline silicon should be taken into account, and a reasonable wavelength λ_n will be chosen. The peak energy among the terrestrial solar spectrum occur in 0.5um, while the peak of relative spectrum response of silicon cells is in the range 0.8-0.9um wavelength, so the wavelength range of the best anti-reflection is in 0.5-0.7um.

In the actual processes of crystalline silicon solar cells, commonly used anti-reflective materials are TiO_2, SiO_2, SiN_x, MgF_2, ZnS, Al_2O_3, etc. Their refractive indexes were listed in Table 1. Their thicknesses are generally about 60-100nm. Chemical vapor deposition (CVD), plasma chemical vapor deposition (PECVD), spray pyrolysis, sputtering and evaporation techniques can be used to deposit the different anti-reflection film.

Materials	Refraction index n
MgF_2	1.38
SiO_2	1.46
Al_2O_3	1.76
Si_3N_4	2.05
Ta_2O_5	2.2
ZnS	2.36
SiOx	1.8-1.9
TiO_2	2.62

Note: The wavelength 590nm (the corresponding energy is 2.1eV) was used in calibration.

Table 1. The refractive index of common anti-reflective materials [Markvart & Castner, 2009]

Among all antireflection coatings, $TiO_x(x \leq 2)$ is one of commonly used antireflection coatings in preparation of crystalline silicon solar cells. This film is usually used as an ideal antireflection coating (ARC) for its high refractive index, and its transparent band center coincides with visible spectrum of sunlight well. And silicon nitride (SiN_x) is another commonly used ARC. Because SiN_x film has good insulating ability, density, stability and masking ability for the impurity ions, it has been widely used in semiconductor production as an efficient surface passivation layer. And in the preparation process of SiN_x coating, it can be easily achieved that the reflection-passivation dual effect, which will improve the conversion efficiency of silicon solar cells significantly. Therefore, since the 90s of the 20th century, the use of SiN_x thin film as antireflection coating has become research and application focus.

3.2 Optimization of the antireflection coating

When conducting coatings optimization design, generally the following assumptions were assumed [Wang, 2001]: 1) The film is an isotropic optical media, and its dielectric properties can be characterized by the refractive index n, where n is a real number. For metals and semiconductors, their dielectric properties can be represented by the complex refractive index N = n-jk (or optical admittance), where N is a plural, and its real part n still represents refractive index, imaginary part k is the extinction coefficient, j is imaginary unit. 2) Two adjacent media was separated with an interface, and the refractive index occurs on both sides change discontinuously. 3) Except the interface, the variation of the refractive index along the film thickness direction is continuous; 4) Films can be separated by two parallel planes, and it is assumed to be infinite in horizontal direction. The thickness of the film has the same magnitude with the light wavelength; 5) The incident light is a plane wave.

In the design of multi-layer coating, the main parameters of the coating structure are: the thickness of each layer d_1, d_2, ...,d_k; incident media, refractive indexes of each layer and the substrate n_0, n_1 ... n_k; light incidence angle θ and wavelength λ. The optical properties of the coating, such as the reflectivity R, depend on these structural parameters. In general, the spectral distribution of incident light is known, so the desired reflectivity R can be achieved by adjusting the values of n_i, d_i (i = 1,2, ... k) and so on.

Fig.7 shows the typical reflectivity curves for single and double layer antireflection coating under normal incidence. We can find the curve shapes in Fig.7(a) and Fig.7(b) are different. The reflectivity curve for single-layer ARC is V-shape, which means the minimum reflectivity only can be achieved in one specific wavelength. If the incident wavelength is far

from this wavelength, the reflectivity increases very much. While the reflectivity curve for double ARC is W-shape. This means that the reflectivity reaches the minimum in two specific wavelengths, which is helpful to suppress the reflectivity in the range 300-1200nm. It is clear from Fig.7 that the antireflection effect of double layer ARC is better than that of single layer ARC.
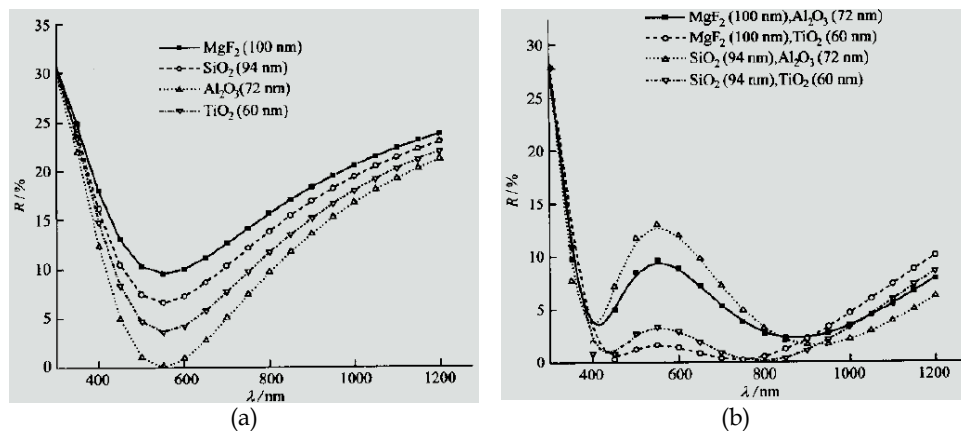

Fig. 7. The typical reflectivity curves for single and double layer antireflection coating. [Wang et al., 2004]

Besides the normal incidence, the oblique incidence should also be considered. This is because in the practical application, except for concentrated solar cells, most solar cells are fixed in a certain direction in accordance with local longitude and latitude. In the whole cycle of the sun rising and landing, the antireflection coating is not always perpendicular to the incident light. The incident angle is always changing and this case is known as oblique incidence. When the ARC designed under normal incidence is applied to the oblique incidence, due to the polarization effect, the reflective properties will change dramatically. Therefore, the antireflection coatings used in the wide-angle should be redesigned to meet the needs of all-weather use.

In the case of oblique incidence, for a single-layer system, the reflectivity can be obtained by Fresnel formula; for a multi-layer system, each layer can be represented by an equivalent interface. If the equivalent admittance of the interface is obtained, the reflectivity of the whole system can be acquired. The basic calculation is as follows [Lin & Lu, 1990]:

For m layers coating system, the refractive index and thickness of each membrane material are known as $n_k, d_k (k = 1, 2, ... m)$, respectively. The refractive index of incident medium and the substrate material are n_0, n_{m+1}, respectively. The light incident angle is θ_0. η_k is the optical admittance. The interference matrix for the k-layer is:

$$M_k = \begin{bmatrix} \cos\delta_k & i(\sin\delta_k)/\eta_k \\ i\eta_k \sin\delta_k & \cos\delta_k \end{bmatrix} \tag{1}$$

where $\delta_k = 2\pi n_k d_k \cos\theta_k / \lambda$ $(k = 0, 1...m)$ is the phase thickness of the k-layer.

Then the interference matrix for the whole m layers system is:

$$M = \prod_{k=1}^{m} M_k \tag{2}$$

In the case of oblique incidence, the admittance values of s polarization and p polarization are different. For the number k layer, they are:

$$\eta_k = \begin{cases} n_k/\cos\theta_k & p \text{ component} \\ n_k \cos\theta_k & s \text{ component} \end{cases} \tag{3}$$

Where θ_k can be given by the Snell law,

$$n_0 \sin\theta_0 = n_k \sin\theta_k, k = 1,2....m, m+1 \tag{4}$$

The expression $Y = C/B$ is the admittance for combinations of multi-layer coatings and the substrate, and B, C were determined by:

$$\begin{bmatrix} B \\ C \end{bmatrix} = M \begin{bmatrix} 1 \\ \eta_{m+1} \end{bmatrix} \tag{5}$$

Where η_{m+1} is the admittance of the substrate layer.

The energy reflectivity R of the thin film system is:

$$R = \left| \frac{1 - Y/\eta_0}{1 + Y/\eta_0} \right|^2 \tag{6}$$

For the R_s component, the Y, η_0 values in above expression should be replaced by Y_s, η_{0s}. For the R_p component, the corresponding Y, η_0 should be substituted by Y_p, η_{0p}. The total energy reflectivity R is:

$$R = \frac{R_s + R_p}{2} \tag{7}$$

The reflectivity R of the whole system depends on the structural parameters of each layer. Since the spectral response of silicon ranges from 300 to 1200nm, so only incident light in the 300-1200nm wavelength range is considered. Taking into account the inconsistent between the solar spectrum and the spectral response curve of silicon, the evaluation function is chosen as:

$$F = \frac{\int_{0.3}^{1.2} S(\lambda) SR(\lambda) R(\lambda) d\lambda}{\int_{0.3}^{1.2} S(\lambda) SR(\lambda) d\lambda} \tag{8}$$

where $S(\lambda), SR(\lambda)$ and $R(\lambda)$ represent the spectral distribution of the sun, the spectral response of silicon and the reflectivity of the antireflection coating in the specific wavelength, respectively. So the weighted average reflectivity F can be calculated within the entire solar spectrum.

3.3 The optimization results

Fig.8 (a), (b), (c), (d) show the results of SiN_x/SiO_2 ARC when 15°, 30°, 45°, 60° were selected as the optimal angles, where the angles marked in the figure are the incident angles. It can be seen from Fig.8 (a) that the reflectivity is too high when the incident angle is large, especially for the longer wavelength range. And comparing the results of the case 60° and 15°, we can find that the 60° optimization can significantly reduce the long-wavelength reflectivity within the 10%, but the reflectivity rises in short-wave area inevitably, which inhibits the absorption of high-energy photons in the solar spectrum. While optimization with 30° shows a good antireflection property. Under this case when the incident angles range from 0° to 45°, the reflectivity curve is relatively stable; even for the 60° incident angle, the reflectivities in short wavelength and long wavelength still maintain below 15%. The optimization results of 45° is similar with those of 60°, the reflectivity for long wavelength under large incident angle is lower, but for small angle case, the reflectivity for short wavelength is too high.
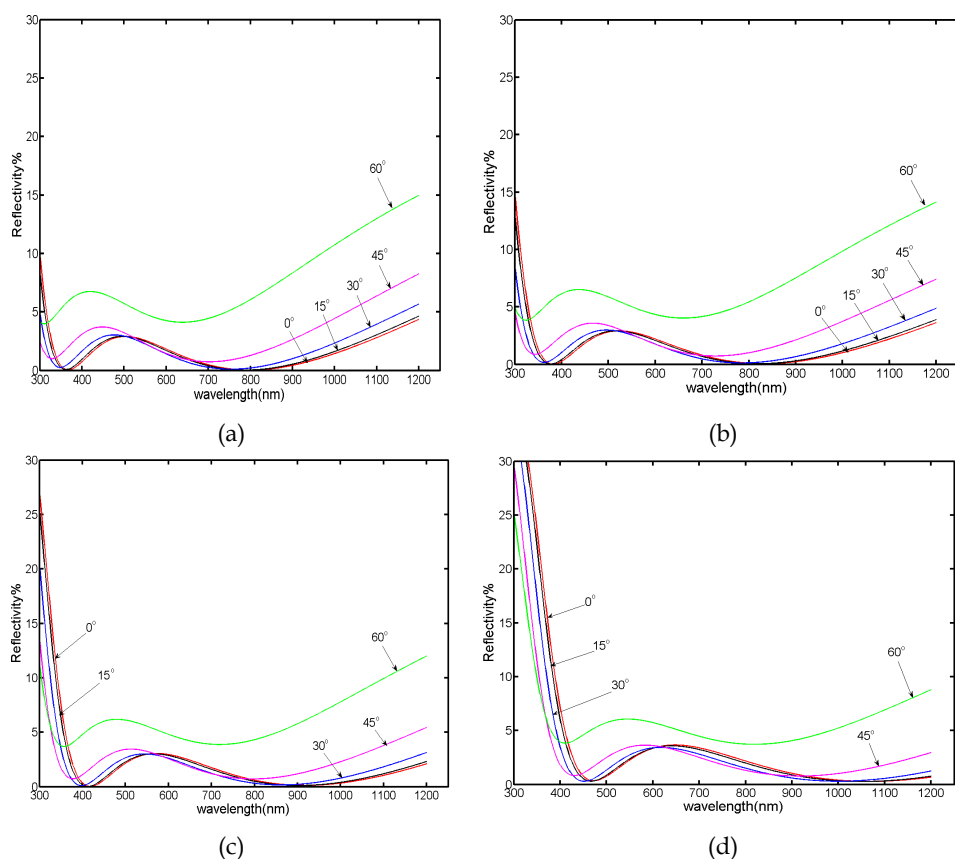

Fig. 8. Under different optimal angles, the reflectivities of optimal SiN_x/SiO_2 ARC vary with the incident angles and wavelength. The different optimal angles equal to
(a) 15°; (b) 30°; (c) 45°; (d) 60°, respectively.[Chen & Wang, 2008]

To further comparing the impact of the optimal angles on the antireflection, combining the intensity distribution of the solar spectrum and spectral response of silicon solar cells, Fig. 9 shows the variation of the weighted average reflectance F with the incident angle. It can be seen from Fig. 9 that if 0° or 15° was selected as an optimal angle, F is just low in small incident angle, with the incident angle increases, F increases rapidly; and if 45° or 60° was used as an optimal angle, although F is low for the large angle, but F is higher in small angle range, especially for 60° case. The value of F is more than 1 percentage point higher than that of 0° in small-angle region. These suggest that if the large angle is selected as the optimal angle, a good anti-reflection effect can't be achieved for the small incident angle. And if 30° is selected, it is clear from the figure that this angle has the minimum average F in this range, so 30°is the best optimization angle.
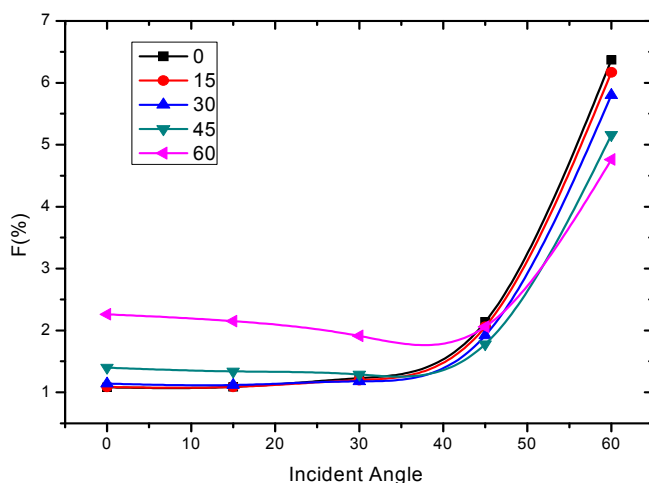

Fig. 9. Weighted average reflectance of double-layer anti-reflection coatings versus different incident angles.[Chen & Wang, 2008]

In conclusion, in practical applications, the oblique incidence is a more common situation. In the oblique incidence case, 30° is the best degree for designing and optimizing ARC.

4. Surface Plasmons [Atwater & Polman, 2010; Pillai et al., 2007]

For thin-film silicon solar cells, the Si absorber has a thickness on the order of only a few micrometers and is deposited on foreign substrates such as glass, ceramics, plastic, or metal for mechanical support. However, the efficiency of such silicon thin-film cells at the moment are low compared to wafer-based silicon cells because of the relatively poor light absorption, as well as high bulk and surface recombination. Fig.10 shows the standard AM1.5 solar spectrum together with a graph that illustrates what fraction of the solar spectrum is absorbed on a single pass through 2-um-thick crystalline Si film. Clearly, a large fraction of the solar spectrum, in particular in the intense 600-1100nm spectral range, is poorly

absorbed. This is the reason that conventional wafer-based crystalline Si solar cells have a much larger thickness of typically 180-300um.
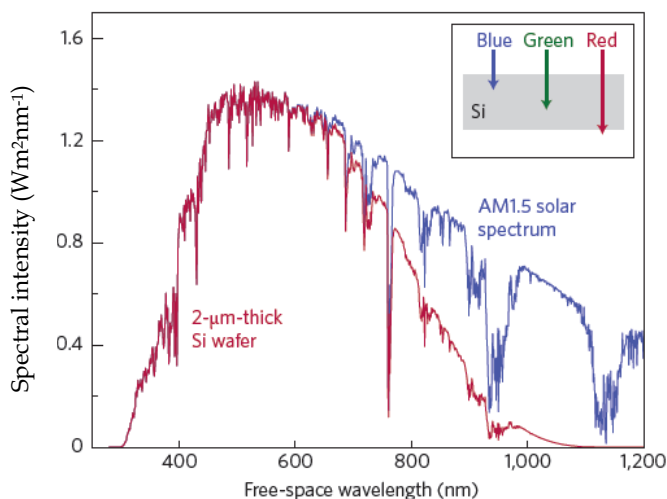

Fig. 10. AM1.5 solar spectrum, together with a graph that indicates the solar energy absorbed in a 2um-thick crystalline Si film (assuming single-pass absorption and no reflection). [Atwater & Polman, 2010]

Because thin-film solar cells are only a few microns thick, standard methods of increasing the light absorption, which use surface textures that are typically around 10 microns in size, cannot be used. Plasma etching techniques, which can be used to etch submicron-sized feature, can damage the silicon, thereby reducing the cell efficiency. Another alternative to direct texturing of Si is the texturing of the substrate. However, this also results in increased recombination losses through increased surface area. Though in practice it has been experimentally proven to be very difficult to reduce recombination losses beyond a certain limit, theoretically energy conversion efficiency of above 24% even for 1um cells can be achieved. This highlights the need to incorporate better light-trapping mechanisms that do not increase recombination losses in thin-film solar cells to extract the full potential of the cells. A new method of achieving light trapping in thin-film solar cells is the use of plasma resonances in metal.

The electromagnetic properties of metal particles have been known for a long time since the work of Wood and Ritchie, but there has been renewed interest in recent years following the development of new nanofabrication techniques which makes it easy to fabricate these nanostructures. Plasmons can exist in bulk, can be in the form of propagating waves on thin metal surface or can be localized to the surface. So the plasmons are termed bulk plasmons, surface plasmon polariton (SPP) and localized surface plasmons (LSP) respectively. Bulk plasmons are studied using electron or x-ray spectroscopy. The excitation of bulk plasmons using visible light is difficult.

Surface Plasmon polaritions (SPPs) are combined excitations of the conduction electrons and a photon, and form a propagating mode bound to the interface between a thin metal and a

dielectric travelling perpendicular to the film plane. This phenomenon only occur at the interface between metals and dielectrics where the Re(ε) (where ε is the dielectric function) have opposite signs, and decay exponentially with distance from the interface, as shown in Fig.11.
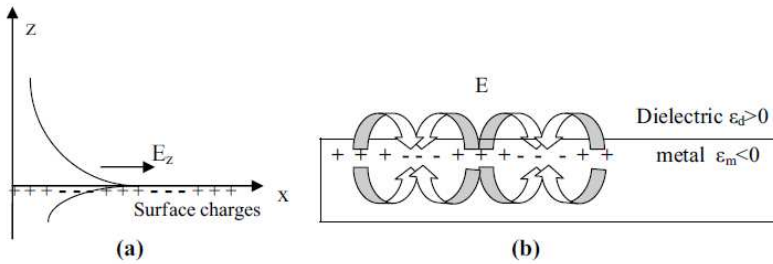

Fig. 11. (a) Schematic of a surface plasmon at the interface of a metal and dielectric showing the exponential dependence of the field E in the z direction along with charges and (b) electromagnetic field of surface plasmons propagating on the surface in the x direction. [Pillai, 2007]

According the theory, the propagating waves can travel up to 10-100um in the visible for silver owing to its low absorption losses and can increase up to 1mm in the near-infrared. Generally the surface plasmon resonant frequency is in the ultra-violet for metals and the infra-red for heavily doped semiconductors.

LSP are collective oscillations of the conduction electrons in metal particles. Movement of the conduction electrons upon excitation with incident light leads to a buildup of polarization charges on the particle surface. This acts as a restoring force, allowing a resonance to occur at a particular frequency, which is termed the dipole surface plasmon resonance frequency. A consequence of surface plasmon excitation in the enhancement of the electromagnetic field around the vicinity of the particles is shown in Fig.12.
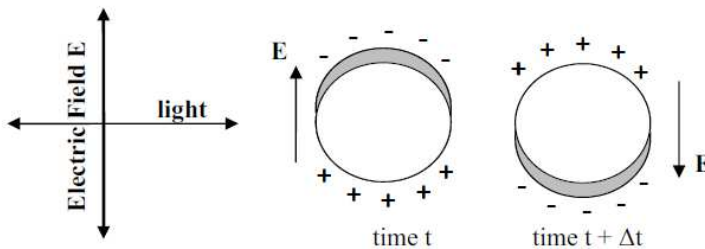

Fig. 12. Incident light excites the dipole localized surface Plasmon resonance on a spherical metal nanoparticle. [Pillai, 2007]

By proper engineering of this metallodielectric structures, light can be concentrated and "folded" into a thin semiconductor layer, thereby increasing the absorption. Both local surface plasmons excited in metal nanoparticles and surface plasmons polaritions propagating at the metals/semiconductor interface are of interest.

Plasmonic structures can offer at least three ways of reducing the physical thickness of the photovoltaic absorber layer while keeping their optical thickness constant, as shown in Fig.13. First, metallic nanoparticles can be used as subwavelength scattering elements to couple and trap freely propagating plane waves from the Sun into an absorbing semiconductor thin film, by folding the light into a thin absorber layer. Second, metallic nanoparticles can be used as subwavelength antenna in which the plasmonic near-field is coupled to the semiconductor, increasing its effective absorption cross-section. Third, a corrugated metallic film on the back surface of a thin photovoltaic absorber layer can couple sunlight into SPP modes supported at the metal/semiconductor interface as well as guided modes in the semiconductor slab, whereupon the light is converted to photocarrier in the semiconductor.
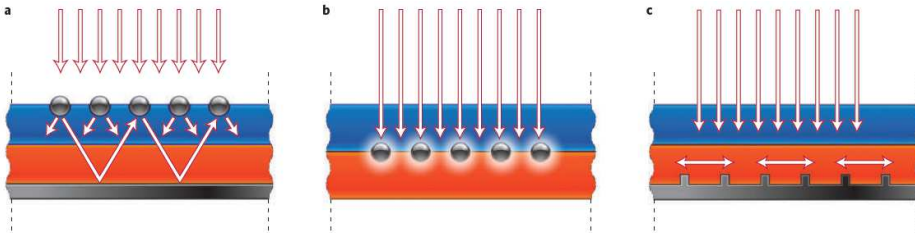

Fig. 13. Plasmonic light-trapping geometric for thin-film solar cells.[Atwater & Polman, 2010]

4.1 Light scattering using particle plasmons

Incident light that is in the region of the resonance wavelength of the particles is strongly scattered or absorbed, depending on the size of the particles. The extinction of the particle is defined as the sum of the scattering and absorption. For small particles in the quasistatic limit, the scattering and absorption cross section are given by [Bohren, 1983; Bohren & Huffman, 1998]

$$C_{sat} = \frac{1}{6\pi}\left(\frac{2\pi}{\lambda}\right)^4 |\alpha|^2$$

and

$$C_{abs} = \frac{2\pi}{\lambda}\text{Im}[\alpha]$$

Here, α is the polarizability of the particle, given by

$$\alpha = 3V\frac{(\varepsilon - 1)}{(\varepsilon + 2)}$$

for a small spherical particle in vacuum, where V is the volume of the particle and ε is the permittivity of the metal. The scattering efficiency Q_{sca} is given by $Q_{sca} = C_{sca}/\pi r^2$, where

πr^2 is the geometric cross section of the particle. Near the surface plasmon resonance, light may interact with the particle over a cross-sectional area larger than the geometric cross section of the particle because the polarizability of the particle becomes very high in this frequency range [Bohren, 1983]. Metals exhibit this property due to excitations of surface plasmons at the frequency where $\varepsilon \cong -2$.

Both shape and size of metal nanoparticles are key factors determining the incoupling efficiency [Pillai & Green, 2010]. This is illustrated in Fig.14a, which shows that smaller particles, with their effective dipole moment located closer to the semiconductor layer, couple a large fraction of the incident light into the underlying semiconductor because of enhanced near-field coupling. Indeed, in the limit of a point dipole very near to a silicon substrate, 96% of the incident light is scattered into the substrate, demonstrating the power of the particle scattering technique. Fig.14b shows the path-length enhancement in the solar cells derived from Fig.14a using a simple first-order scattering model. For 100-nm-diameter Ag hemispheres on Si, a 30-fold enhancement is found. These light-trapping effects are most pronounced at the peak of the plasmon resonance spectrum, which can be tuned by engineering the dielectric constant of the surrounding medium. For example, small Ag or Au particles in air have plasmon resonances at 350nm and 480nm respectively; they can be redshifted in a controlled way over the entire 500-1500nm spectral range by (partially) embedding them in SiO_2, Si_3N_4 or Si, which are all standard materials in solar cell manufacturing. The scattering cross-sections for metal nanoparticle can be as high as ten times the geometrical area, and a nearly 10% coverage of the solar cell would sufficient to capture most of the incident sunlight into plasmon excitations.
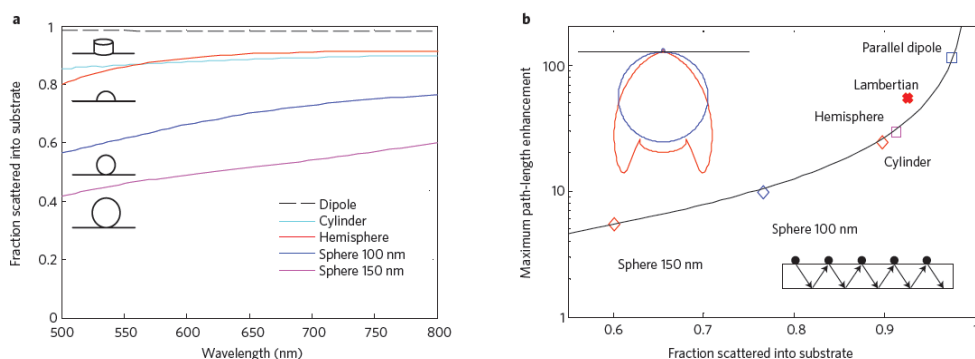

Fig. 14. Light scattering and trapping is very sensitive to particle shape. a. Fraction of light scattered into the substrate, divided by total scattered power, for different sizes and shapes of Ag particles on Si. Also plotted is the scattered fraction for a parallel electric dipole that is 10nm from a Si substrate. b. Maximum path-length enhancement for the same geometries as in left figure at a wavelength of 800nm. Absorption within the particles is neglected for these calculations and an ideal rear reflector is assumed. The line is a guide for eyes. Insets (top left) angular distribution of scattered power for a parallel electric dipole that is 10nm above a Si layer and Lambertian scatter; (bottom-right) geometry considered for calculating the path length enhancement. [Catchpole & Polman, 2008]

4.2 Light concentration using particle plasmons.

An alternative use of resonant plasmon excitation in thin-film solar cells is to take advantage of the strong local field enhancement around the metal nanoparticle to increase absorption in a surrounding semiconductor material. The nanoparticles then act as an effective 'antenna' for the incident sunlight that stores the incident energy in a localized surface plasmon mode (Fig.13b). This works particularly well for small (5-20nm diameter) particles for which the albedo is low. These antennas are particularly useful in materials where the carrier diffusion lengths are small, and photocarriers must be generated close to the collection junction area.

Several examples of this concept have recently appeared that demonstrate enhanced photocurrents owing to the plasmonic near-field coupling. Enhanced efficiencies have been demonstrated for ultrathin-film organic solar cells doped with very small (5nm diameter) Ag nanoparticles. An increase in efficiency by a factor of 1.7 has been shown for organic bulk heterojunction solar cells. Dye-sensitized solar cells can also be enhanced by embedding small metal nanoparticles. Also, the increased light absorption and increased photocurrent also reported for inorganic solar cells, such as CdSe/Si heterojunction, Si and so on. The optimization of the coupling between plasmons, excitons and phonons in metal-semiconductor nanostructures is a rich field of research that so far has not received much attention with photovoltaics in mind.

4.3 Light trapping using SPPs

In a third plasmonic light-trapping geometry, light is converted into SPPs, which are electromagnetic waves that travel along the interface between a metal back contact and the semiconductor absorber layer, as shown in Fig.13c. Near the Plasmon resonance frequency, the evanescent electromagnetic SPP fields are confined near the interface at dimensions much smaller than the wavelength. SPPs excited at the metal/semiconductor interface can efficiently trap and guide light in the semiconductor layer. In this geometry the incident solar flux is effectively turned by 90°, and light is absorbed along the lateral direction of the solar cell, which has dimensions that are orders of magnitude larger than the optical absorption length. As metal contacts are a standard element in the solar-cell design, this plasmonic coupling concept can be integrated in a natural way.

At frequencies near plasmon resonance frequency (typically in the 350-700nm spectral range, depending on metal and dielectric) SPPs suffer from relatively high losses. Further into the infrared, however, propagation lengths are substantial. For example, for a semi-infinite Ag/SiO_2 geometry, SPP propagation lengths range from 10 to 100um in the 800-1500nm spectral range. By using a thin-film metal geometry the plasmon dispersion can be further engineered. Increased propagation length comes at the expense of reduced optical confinement and optimum metal-film design thus depends on the desired solar-cell geometry. Detailed accounts of plasmon dispersion and loss in metal-dielectric geometries are found in references [Berini, 2000; Berini, 2001; Dionne et al., 2005; Dionne et al., 2006].

The ability to construct optically thick but physically very thin photovoltaic absorbers could revolutionize high-efficiency photovoltaic device designs. This becomes possible by using light trapping through the resonant scattering and concentration of light in arrays of metal nanoparticles, or by coupling light into surface plasmon polaritons and photonic modes that propagate in the plane of the semiconductor layer. In this way extremely thin photovoltaic absorber layers (tens to hundreds of nanometers thick) may absorb the full solar spectrum.

5. References

Atwater, H. A. & Polman, A. (2010). Plasmonics for improved photovoltaic devices. *Nature Materials*, vol. 9, pp.205–213, ISSN 1476-1122

Basu, P.K.; Pujahari, R.M; Harpreet K. et al. (2010). Impact of surface roughness on the electric parameters of industrial high efficiency NaOH-NaOCl textured multicrystalline silicon solar cell, *Solar Energy*, vol.84, No.9, pp.1658-1665, ISSN 0038-092X

Berini P, (2000). Plasmon-polariton waves guided by thin lossy metal films of finite width: bound modes of symmetric structures. *Phys. Rev.B*, Vol.61, pp.10484-10503, ISSN 1098-0121

Berini P, (2001). Plasmon-polariton waves guided by thin lossy metal films of finite width: bound modes of asymmetric structures. *Phys. Rev.B*, Vol.63, pp.125417, ISSN 1098-0121

Bohren C.F., (1983). How can a particle absorb more than the light incident on it? *Am. J.Phys.* vol.51, No.4, pp.323-327, ISSN 0002- 9483

Bohren C.F. & Huffman D.R., (1998). *Absorption and scattering of light by small particles*, Wiley Interscience, ISBN 0471293407, New York

Catchpole K. R. & Polman A., (2008). Plasmonic solar cells. *Optics Express*, vol.16, No.26, pp.21793-21800, ISSN 1094-4087

Catchpole K.R. & Polman A., (2008). Design principles for particle plasmon enhanced solar cells. *Appl. Phys. Lett.* Vol.93, pp.191113-1-191113-3, ISSN 0003-6951

Chen F.X. & Wang L.S., (2008). Optimized Design of Antireflection Coating for Silicon Solar Cells with Board Angle Usage, *Acta Energiae Solaris Sinica*, vol.29, pp.1262-1266, ISSN 0254-0096

Derkacs D., Lim S. H., Matheu P., et al. (2006). Improved performance of amorphous silicon solar cells via scattering from surface plasmon polaritons in nearby metallic nanoparticles. *Appl. Phys. Lett.*, vol.89, pp. 093103-1-093103-3, ISSN 0003-6951

Dionne J.A, Sweatlock I, Atwater H.A & Polman, A. (2005). Planar plasmon metal waveguides: frequency-dependent dispersion, propagation, localization, and loss beyond the free electron model. *Phys. Rev.B*, vol.72, pp.075405, ISSN 1098-0121

Dionne J.A, Sweatlock I, Atwater H.A & Polman A. (2006). Plasmon slot waveguides: towards chip-scale propagation with subwavelength-scale localization. *Phys. Rev.B*, vol.73, pp.035407, ISSN 1098-0121

Fesquet L, Olibet S, Damon-Lacoste J et al. (2009). Modification of textured silicon wafer surface morphology for fabrication of heterojunction solar cell with open circuit voltage over 700mV. *34th IEEE Photovoltaic Specialists Conference (PVSC)*, ISBN 978-1-4244-2950-9, Philadelphia, June, 2009

Gangopadhyay U, Dhungel S.K, Basu P.K, et al. (2007). Comparative study of different approaches of multicrystalline silicon texturing for solar cell fabrication. *Solar Energy Materials and Solar Cells*, vol.91, No.4, pp.285-289, ISSN 0927-0248

Geng Xue-Wen, Li Mei-Cheng & Zhao Lian-Cheng, (2010). Research development of light trapping structures for thin-film silicon solar cells, *Journal of Function Materials*, vol.41, No.5, pp.751-754, ISSN 1001-9731

Inomata Y., Fukui K. & Shirasawa K., (1997). Surface texturing of large area multi-crystalline silicon solar cells using reactive ion etching method. *Solar Energy Materials and Solar Cells*, vol. 48, pp.237-242, ISSN 0927-0248

Ju M, Gunasekaran M, Kim K, et al. (2008). A new vapor texturing method for multicrystalline silicon solar cell applications, *Materials Science and Engineering B: Solid-State Materials for Advanced Technology*, vol.153, pp.66-69, ISSN 9215-5107

Kuo Mei-Ling, Poxson David J, Kim Yong Sung et al. (2008). Realization of a near-perfect antireflection coating for silicon solar energy utilization, *Optics Letters*, vol.33, No.21,pp.2527-2529, ISSN 0146-9592

Li Qun Wu, Yan Chao & Jian Shao, (2011). Texturing of multi-crystalline silicon wafers through ionized bubble for solar cell fabrication, *Advanced Materials Research*, vol.216, pp. 592-595, ISSN 1022-6680

Lin Y.C. & Lu W.Q., (1990). *Principles of Optical Thin Films*, National Defense Industry Press, ISBN 978-7-118-00543-1, China:Beijing

Maria Losurdo, Maria M. Giangregorio, Giuseppe V. Bianco, et al. (2009). Enhanced absorption in Au nanoparticles/a-Si:H/c-Si heterojunction solar cells exploiting Au surface plasmon resonance. *Solar Energy Materials & Solar Cells,* vol.93, pp.1749-1754, ISSN 0927-0248

Markvart Tom & Castner Luis, (2009). *Solar cells: Materials, Manufacture and Operation,* China Machine Press, ISBN 978-7-111-26798-0, China:Beijing

Meng F.Y., (2001). Grain boundary theory and photovoltaic characteristics of solar cell on polycrystalline silicon material, *Ph.D thesis,* Shanghai Jiaotong University, Shanghai, China

Moulin E., Sukmanowski J., Luo P., et al, (2008). Improved light absorption in thin-film silicon solar cells by integration of silver nanoparticles. *J. Non-Cryst. Solids,* vol.354, pp.2488–2491, ISSN: 0022-3093

Nakayama K., Tanabe K. & Atwater H.A., (2008). Plasmonic nanoparticle enhanced light absorption in GaAs solar cells. *Appl. Phys. Lett.*, vol.93, pp.121904-1–121904-3, ISSN 0003-6951

Pillai S., (2007). Surface plasmons for enhanced thin-film silicon solar cells and light emitting diodes, *Ph.D thesis,* University of NewSouth Wales, Sydney, Australia

Pillai S., Catchpole K. R., Trupke T., et al. (2007). Surface plasmon enhanced silicon solar cells. *J.Appl. Phys.* Vol.101, pp.093105-1-093105-8, ISSN 0021-8979

Pillai S. & Green M.A., (2010). Plasmonics for photovoltaic applications. *Solar Energy Materials and Solar Cells,* Vol.94, No. 9, pp.1481-1486, ISSN 0927-0248

Wang H.Y., (2005), The research on light-trapping materials and structures for silicon-based solar cells. *Ph.D thesis*, Zhengzhou University, Zhengzhou, China

Wang Y.D., (2001). Study on optical properties of solar cells, *Ph.D thesis,* Shanghai Jiaotong University, Shanghai, China

Wang W.H., Li H.B. & Wu D.X., (2004). Design and analysis of anti-reflection coating for solar cells, *Journal of Shanghai University (Nature Science)*, vol.10, No.1, pp.39-42, ISSN 1007-2861

Xiong C., Yao R.H. & Gen K.W., (2010). Two low reflectance of triple-layer broadband antireflection coating for silicon solar cells. *Proceeding on 10th IEEE International Conference on Solid-State and Integrated Circuit Technology*, ISBN 978-1-4244-5798-4, Shanghai, China, Nov.2010

Yang Deren. (2010). *Materials for solar cells*, Chemical Industry Press, ISBN 978-7-5025-9580-7, China:Beijing
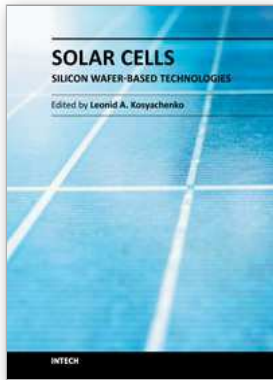
Solar Cells - Silicon Wafer-Based Technologies

Edited by Prof. Leonid A. Kosyachenko

The third book of four-volume edition of 'Solar Cells' is devoted to solar cells based on silicon wafers, i.e., the main material used in today's photovoltaics. The volume includes the chapters that present new results of research aimed to improve efficiency, to reduce consumption of materials and to lower cost of wafer-based silicon solar cells as well as new methods of research and testing of the devices. Light trapping design in c-Si and mc-Si solar cells, solar-energy conversion as a function of the geometric-concentration factor, design criteria for spacecraft solar arrays are considered in several chapters. A system for the micrometric characterization of solar cells, for identifying the electrical parameters of PV solar generators, a new model for extracting the physical parameters of solar cells, LBIC method for characterization of solar cells, non-idealities in the I-V characteristic of the PV generators are discussed in other chapters of the volume.

How to reference

In order to correctly reference this scholarly work, feel free to copy and paste the following:

Fengxiang Chen and Lisheng Wang (2011). Light Trapping Design in Silicon-Based Solar Cells, Solar Cells - Silicon Wafer-Based Technologies, Prof. Leonid A. Kosyachenko (Ed.), ISBN: 978-953-307-747-5, InTech, Available from: http://www.intechopen.com/books/solar-cells-silicon-wafer-based-technologies/light-trapping-design-in-silicon-based-solar-cells

INTECH
open science | open minds